Effect of Plasmonic Nanostructures on the Optical Properties of CH₃NH₃PbI Perovskite Films

Dmitriy Afanasyev[1], Niyazbek Ibrayev[1] and Nurxat Nuraje[2]*

[1]Institute of Molecular Nanophotonics, Buketov Karaganda University, Karaganda, Kazakhstan, [2]Department of Chemical and Materials Engineering, School of Engineering and Digital Science, Nazarbayev University, Nur-Sultan, Kazakhstan

This paper investigated the optical properties of both silver island films (SIF) and $CH_3NH_3PbI_3$ perovskite films obtained on the surface of SIF. It was found that the surface morphology of SIF has a substantial effect on the optical density of perovskite films. Furthermore, a significant redshift in the absorption spectrum of the island films was observed when perovskite is deposited on them. The intensity and lifetime of the luminescence of perovskite films on the surface of the island films depend on the wavelength of the exciting light. The results indicate that SIFs not only can be potentially used to increase the intensity of light emitting diodes based on perovskites, but also prolong the lifetime of charge carriers in perovskites, and thus lead to potentially improve the photovoltaic properties of perovskite solar cells.

Keywords: silver island film, localized plasmon resonance, absorption spectra, permittivity, luminescence, organic-inorganic halide perovskite

INTRODUCTION

Recently, researchers became more interested in the study of metal-halide based-perovskites materials, especially from the perspective to use them in perovskite solar cells (PSCs) and light-emitting diodes (LEDs) (Nuraje and Su et al., 2013; Moniruddin et al., 2018; Shandan et al., 2018; Moakhar et al., 2020; Gu et al., 2020). One approach for making the conversion of light energy to electric energy in PSC more efficient and increasing the quantum efficiency of illumination in LEDs is to utilize metal nanostructures with localized surface plasmon resonance (LSPR) in the above devices (Gu et al., 2020; Moakhar et al., 2020). In the presence of plasmonic nanostructures, the electroluminescence efficiency of perovskite LEDs and the conversion efficiency of PSC cells have been increased by 2-fold and by 10–30% respectively (Fu et al., 2017; Han et al., 2019; Moakhar et al., 2020). Furthermore, electron-photon interaction time for a 100 nm thick film of silicon, is 1 fs. On contrary, the electron-photon interaction time is increased to 5–10 fs for the films with addition of surface plasmonic NPs (Schaadt et al., 2005). Another explanation for the increase of the light absorption is ascribed to scattering occurrence by plasmon NPs. Based on the numerical calculations and experimental evidences, a maximum scattering is observed for photons with an energy corresponding to the plasmon resonance energy (Krutyakov et al., 2008). An increase in the degree of scattering can lead to a delay in electro-magnetic radiation in the film and, consequently, an increase in light absorption. Here, it should be noted that the frequency of plasmon resonance is determined by the size and shape of plasmon NPs (Krutyakov et al., 2008). Also, the change of the photocurrent is result of electron emission from plasmon NPs under the influence of light (Protsenko and Uskov, 2012).

Lately, some scientific works indicate that plasmon resonance can increase the rate of exciton dissociation and reduce the rate of exciton recombinationor a number of radiative/non-radiative processes (Wu et al., 2011; Cuiet al., 2016).

In those scientific works, optical spectroscopic technique is a common technique to determine absorption coefficient, optical band gap, the concentration of defects, and diffusion length of charge carriers in organic-inorganic perovskite films. (Xing et al., 2013; Peng et al., 2016; Belykh et al., 2019).

However, laser kinetic spectroscopy techniques (including time-resolved photoluminescence and transient absorption spectroscopy) are the most useful tools to investigate charge transfer features of the PSC. They are able to estimate the lifetime of charge carriers, determine the efficiency of charge transfer from a perovskite film to semiconductor layers with n—and p—type conductivity, and measure the concentration of defects in perovskite films (Xing et al., 2014; Peng et al., 2016; Pydzin´ska et al., 2016).

Despite the numerous amounts of studies in the plasmonic solar cells (Catchpole and Polma, 2008; Stratakis and Kymakis 2013; Chan et al., 2017), few studies committed to the mechanistic study on the effect of plasmonic nanoparticles on solar energy conversion performance of PSC. First study on plasmonic perovskite solar cell was carried out by the Snaith group in 2013 (Zhang et al., 2013). Adding plasmonic NPs to PSC increases the absorption rate of the perovskite materials in the near field of plasmon nanoparticles due to the prolonged electron-photon interaction time. Investigation of the LSPR effect on photophysical processes in perovskite films was carried out by Bayles et al. (Bayles et al., 2020; Li et al., 2020). Design of the localized LSPR in core-shell nanoparticles was allowed to raise the light absorption in the perovskite films. Also, two fold increase of the perovskite photoemission efficiency was obtained. Using of finite-difference time-domain (FDTD) simulation accurately described the results of absorption spectra of perovskite films. The above results were obtained for only core-shell structure of metal and silicon dioxide or nanospherical/cubic particles. However, one possible way to study the influence of localized plasmon resonance on the optical properties of perovskite films is to create island films of metals, in particular, silver films (Haes et al., 2006; Zhao et al., 2007; Toropov et al., 2014) since the nanoisland metals not only provide better anisotropic optical properties relative to nanospherical particles, but also they can be better controlled via thermal deposition method. Thermal annealing of the silver island films (SIF) proceeds to alter the characteristics of their localized plasmon resonance, leading to subsequent variation in the intensity and shape of the absorption spectra of SIF (Duyne et al., 1993). The change in the size of NPs as a result of thermal annealing makes it possible to determine the main regularities of the influence of metal NPs on the absorption and luminescence of perovskite films. It's known (Khlebtsov, 2008; Krutyakov et al., 2008; Rycenga et al., 2011) that silver has the most intense LSPR among all metals. Therefore the use of Ag NPs can make it possible to investigate the LSPR effect in a wider spectral range, starting from 400 nm.

This paper systematically investigates the influence of silver island films on the optical properties of $CH_3NH_3PbI_3$ perovskite films for the first time. The investigation makes it possible to determine the value of redshift of the absorption spectra of silver island films associated with a change in the permittivity of the medium surrounding silver films. Computer simulation of extinction, absorption and scattering spectra of silver NPs in media with different values made it possible to understand the reasons for such changes. The effect of SIF on the intensity and lifetime of the luminescence of perovskite films is also observed.

EXPERIMENTAL METHODS

Preparation of Silver Island Films
SIFs were prepared by vacuum thermal evaporation of silver nitrate $AgNO_3$ on the cover glass at a residual pressure of P = $2 \cdot 10^{-5}$ mbar. Before the deposition of samples, the surface of the glass substrate was carefully treated in the following way. In brief, the substrates were washed separately in acetone, isopropyl alcohol, and deionized water for 15 min in an ultrasonic bath. Next, the cleaned surface was further treated in an oxygen plasma in the plasma cleaner PDC-002-CE (Harrick Plasma). After the oxygen plasma treatment, the clean glass substrate was used to deposit silver films. The deposition rate of silver films and their thickness were controlled by using a SI-TM108A thickness meter. The thickness of the films was maintained at 5 nm for whole experimental measurements.

To eliminate the variation of the synthesis conditions for growth of the perovskite films, silver film was applied only to half of the glass substrate (**Supplementary Figure S1**; **Supplementary Material (SI)**) and the optical properties of perovskite films were measured from both the glass surface and silver film for each sample.

The properties of localized plasmonic resonance were regulated via annealing the films. Thermal annealing of SIF was carried out in a thermostatically controlled muffle furnace in the air for 10 min at temperatures of 180, 200, 220, 240, 260, 280°C.

Silver island films are susceptible to solvents. Therefore, 200 uL of DMFA was applied to coat the surface of SIF by spin coating each time.

Preparation of Perovskite Layers
Fabrication of $CH_3NH_3PbI_3$ perovskite film was performed on the surface of SIF using a two-step method (Park 2016; Afanasyev et al., 2018). In this approach, a spin-coating method (spin coater, SPIN150i, Netherlands) was applied to spin the solution of PbI_2 on the surface of substrates at a rotation speed of 3,000 rpm. Then, the substrate was further dried at two temperatures 50°C and 100°C stepwise. Next, a solution of methylammonium iodide (CH_3NH_3I) was applied on the top of the dried substrate at the rotation speed of 1,000 rpm. Subsequently the films were heat treated at temperatures of 50°C and 100°C respectively before any characterization or measurements.

All operations related to the synthesis of perovskite films were performed in a glove box under an inert atmosphere (SPECS GB 03-2M, Lomonosov Moscow State University).

Surface Topological Characterization

Microstructures of the synthesized films were studied using a scanning electron microscope (SEM, TESCAN Mira 3). Particle size distributions from SEM-image were estimated by using manual method with ImajeJ 1.50e software from SEM images (Ribeiro et al., 2020). The topological image ofthe silver films was also obtained using an atomic force microscope (AFM, JSPM-5400) in semi–contact mode using cantilevers (NT-MDT, NSG30). The analysis of AFM data was performed using a professionalsoftware (WinspmII Data Processing software). XRD patterns were collected on a Bruker D2 diffractometer.

Optical Measurements

The absorption spectra of films were recorded using an optical spectrophotometer (a Cary 300, Agilent).

Computer simulation of extinction, absorption and scattering spectra of silver NPs in media with different values of the real part of dielectric function of a medium was performed via a special program (Mieplot V.4.6.11 program). The algorithm of numerical calculations is described in detail in Grainger et al. (2004) and Šileikaite et al. (2006).

Luminescence spectra of perovskites were measured using a spectrofluorometer (a Cary Eclipse, Agilent).

The kinetics of photoluminescence of perovskite films was measured using a pulsed spectrofluorometer (Becker & Hickl GmbH) with registration in the time-correlated single photon counting (TCSPC) based on Simple-Tau 150 system.

Luminescence spectra of the samples were collected using pulsed semiconductor lasers at the excitation wavelengths between 488 and 640 nm. Pulse durations with full width at half maximum (FWHM) were 100–150 ps. The lifetime of the films was determined using software for collecting and analyzing SPCM Image data (SPCImage 3.9.4. Data Analysis for Fluorescence Lifetime Imaging Microscopy).

The luminescence lifetime in perovskite films was calculated according to the formula used to approximate the decay kinetics:

$$I(t) = \sum_{n=1}^{3} \left(A_i \, e^{t/\tau_1} \right) \qquad (1)$$

Where,τ_i, A_i—the lifetime and amplitude of each component of the luminescence of the perovskite ($\sum_{i=1}^{3} A_i = 100\%$). The average lifetime of theemissionglow was determined by the formula $\tau_\Sigma = \sum_{i=1}^{3} A_i \tau_i$. In more detail, the method of analyzing kinetic data is given in Afanasyev et al. (2020).

To determine the degree of influence of the silver films on the optical properties of perovskite films, the absorption and luminescence spectra, as well as the luminescence kinetics of the films were measured in parallel with the surface of the silver films and glass for the same sample (**Supplementary Figure S1**; **SI**).

RESULTS AND DISCUSSION

To investigate the effect of metal nanoparticles on the perovskite films, the growth behaviors of silver nanoparticles were investigated first. The thermal evaporation technique was applied in a vacuum environment to generate silver nanoparticles on the glass substrate using source of silver nitrate (AgNO$_3$) precursor. SEM–image of silver films on the surface of the cover glass with and without annealing temperatures of 180, 200, 220, 240, 260, 280°C are shown in **Figure 1**. Silver films before thermal annealing consisted of silver islands with various sizes. The average particle size without annealing is around 25.9 nm with notable variations of size ranges. Both small particles and large particles with sizes over 80 nm are observed as shown in **Figure 1A**. Thermal annealing increases size of NPs by 1.5–2 times. Average diameter for annealing temperatures of 180, 240 and 260°C is equal to 49.8, 51.1, and 48.8 nm, respectively (**Supplementary Figure S2**; **Supplementary Table S1**; **SI**). The s tandard deviation of silver nanoparticle sizes increase with growth in annealing temperature of the samples (**Supplementary Table S1**; **SI**).

Topological images of silver island films annealed at different temperatures were obtained by AFM (**Supplementary Figure S3**; **SI**). The roughness of the silver film's surface depended on the annealing temperature of the films (**Supplementary Table S2**; **SI**). Structures with an average size of 300 nm of an asymmetric shape were formed after deposition the silver film on the glass surface. The surface roughness of the silver film increased in comparison with the surface roughness of the glass (**Supplementary Table S2**; **SI**). After annealing at $T = 180°C$, the properties of silver films change significantly, and spherical nanoparticles are formed on the surface of the substrate. The roughness of the film is gradually increased compared to the roughness of glass and silver film without annealing (**Supplementary Table S2**). Further annealing led to an increase in roughness, but there are no sharp changes in the surface morphology of silver films (**Supplementary Figures S3C–F**; **SI**).

The absorption spectra of silver films are shown in **Figure 2A**. The presence of a wide band with a maximum in the region λ_{max} = 490 nm and a full width at half maximum $FWHM$ = 246 nm was received for silver films obtained directly after deposition (**Supplementary Table S3**; **SI**). A large value of $FWHM$ for the absorption spectrum is associated with variations in the nanoparticles sizes. The annealing of silver films leads to an increase in the optical density of the films D, a blue shift in the absorbance, and a decrease $FWHM$ of the absorption spectrum. The most significant change is observed at the initial annealing temperature of 180°C. At the annealing temperature $T = 240°C$, the plasmon resonance band experiences a blueshift to a maximum of λ_{max} = 426 nm, and also a narrowing of $FWHM$ to 85 nm compared to the plasmon resonance band of the non-annealed silver films. For more information on the effect of the annealing temperature on the optical properties of SIF, see the **Supplementary Table S3** and **SI**.

The effect of DMFA solvent on the optical properties of silver films was studied. **Figure 3** shows the absorption spectra of the films before and after thermal annealing at $T = 220°C$, and the effect of the solvent. After solvent deposition on the anneal silver films, both the value of maximum optical density $\lambda_{Abs_{мач}}$ and
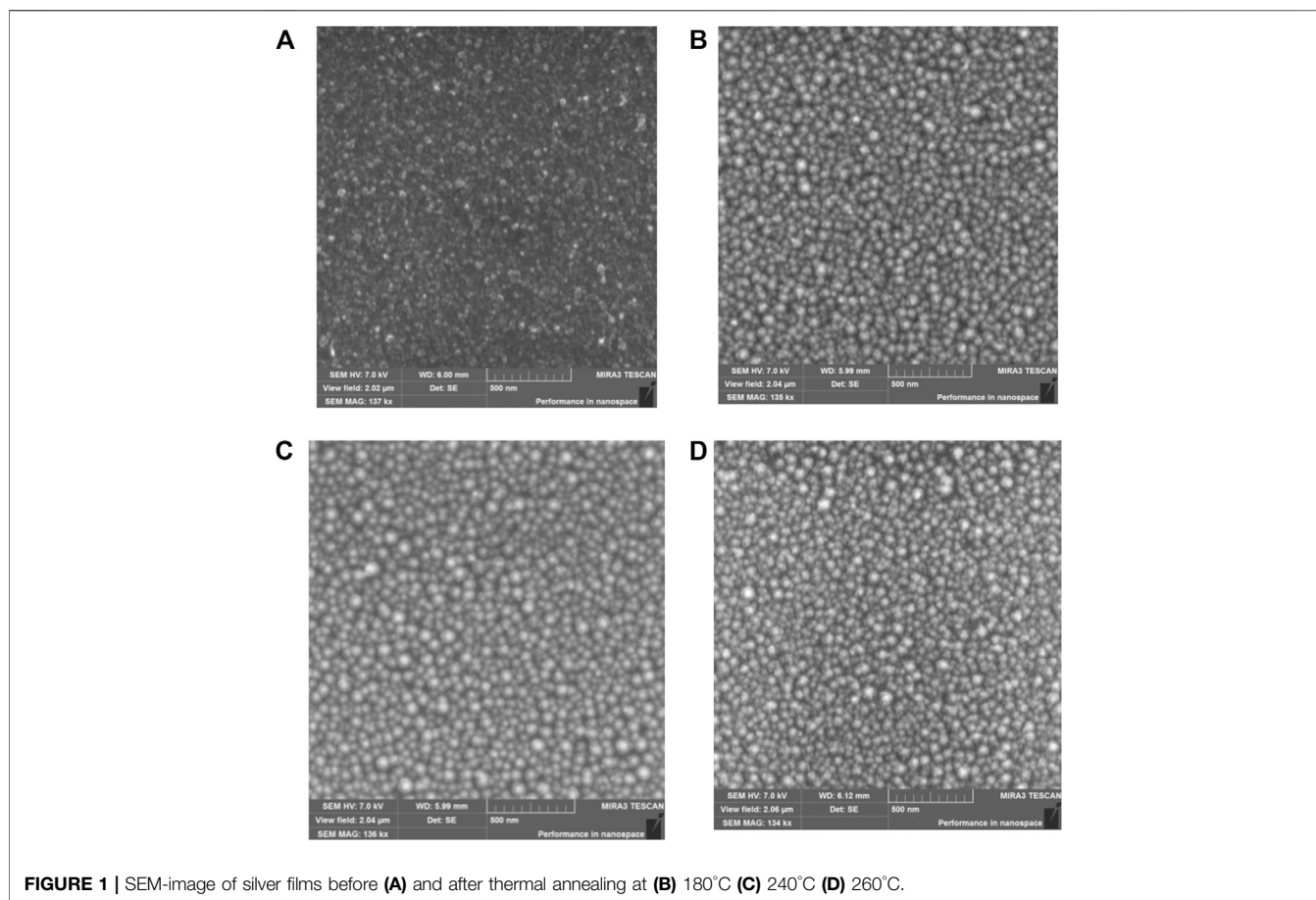
FIGURE 1 | SEM-image of silver films before **(A)** and after thermal annealing at **(B)** 180°C **(C)** 240°C **(D)** 260°C.

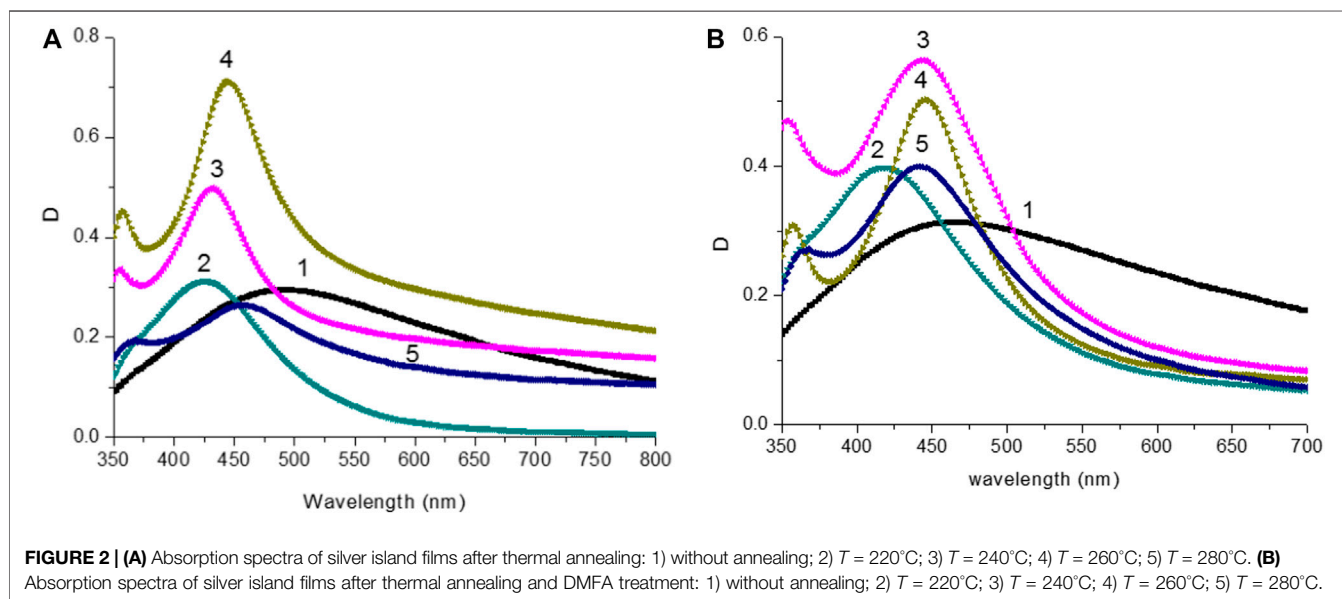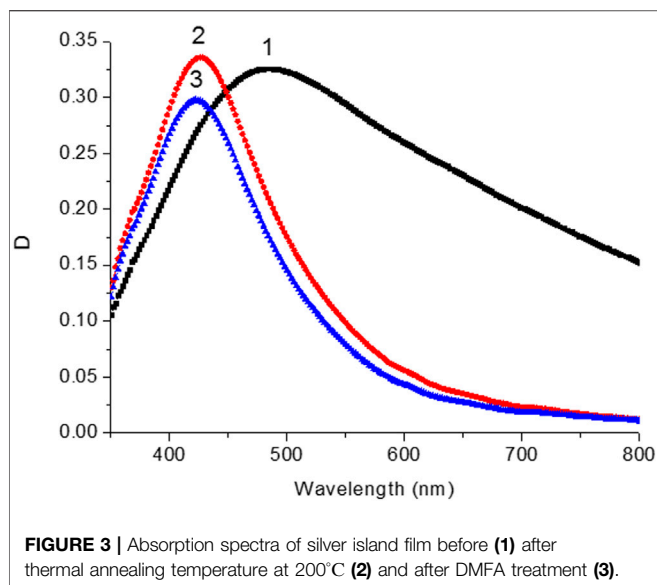**FIGURE 2 | (A)** Absorption spectra of silver island films after thermal annealing: 1) without annealing; 2) T = 220°C; 3) T = 240°C; 4) T = 260°C; 5) T = 280°C. **(B)** Absorption spectra of silver island films after thermal annealing and DMFA treatment: 1) without annealing; 2) T = 220°C; 3) T = 240°C; 4) T = 260°C; 5) T = 280°C.

FWHM of absorption bands (**Supplementary Table S3**; **SI**) were changed. Absorption spectra of SIF with DMFA treatment are shown in **Figure 2B**. Data on the values of $\lambda_{Abs\text{мач}}$, *FWHM* films are reported in **Supplementary Table S3** (**SI**).

The crystallographic identification was conducted using XRD. **Figure 4**, a shows XRD pattern tetragonal symmetry structure for $CH_3NH_3PbI_3$ film (Oku, 2015). Microscopic measurements have shown that the size of $CH_3NH_3PbI_3$ microcrystallites is in the

FIGURE 3 | Absorption spectra of silver island film before **(1)** after thermal annealing temperature at 200°C **(2)** and after DMFA treatment **(3)**.
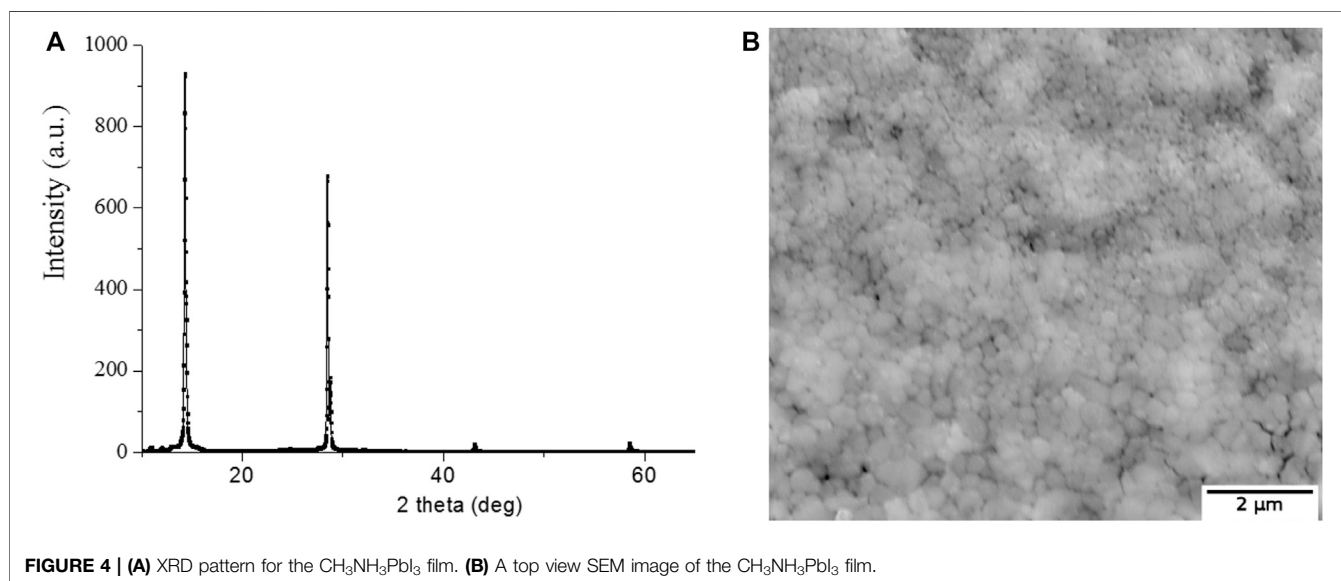
range from 200 to 500 nm (**Figure 4B**). The average thickness of perovskite films was 350 nm.
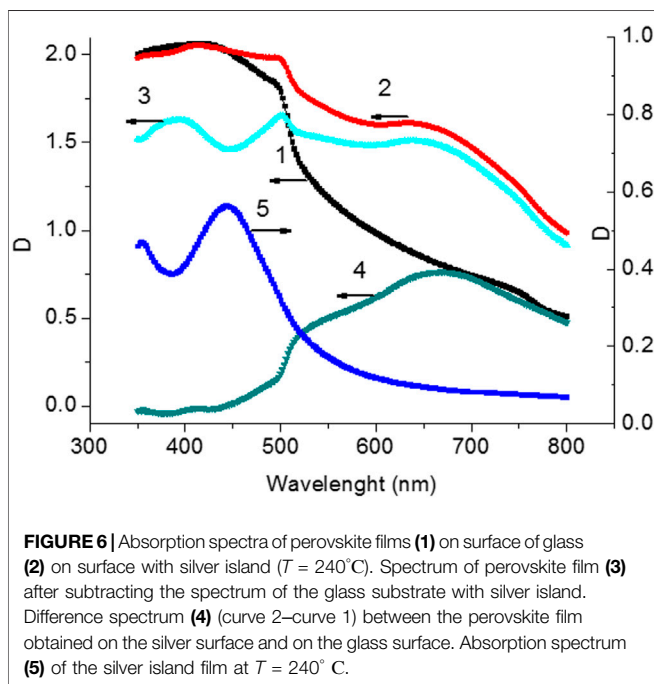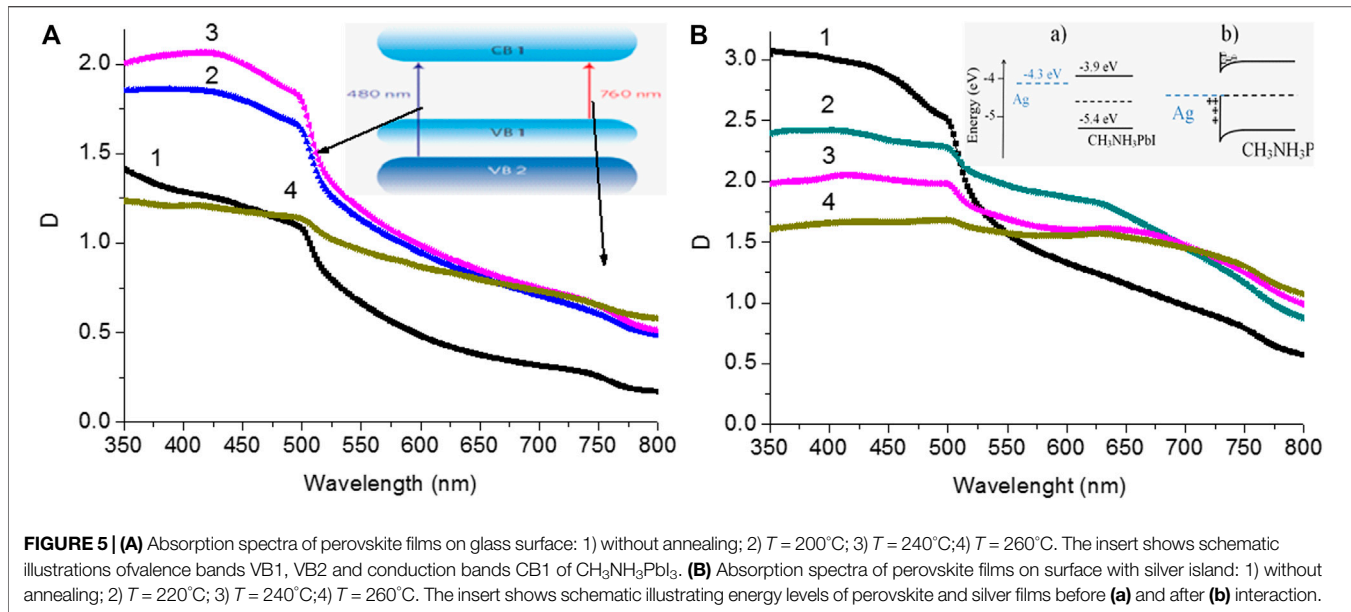
The SIF films processed in DMFA solvent were further used for the synthesis of perovskite films on their surface. Absorption spectra of $CH_3NH_3PbI_3$ films are shown in **Figure 5A**. The absorption spectra correspond to the spectra of $CH_3NH_3PbI_3$were compared with the spectra reported in the literature (Park et al., 2016; Penget al., 2016; Afanasyev and Ibrayev, 2020; Moakharet al., 2020). It was worthwhile to pay attention to two absorption bands in the absorption spectrum which are corresponding to an optical transition of VB2-CB1 (480 nm) and VB1-CB1 (760 nm) (insert of **Figure 5A**) (Cui et al., 2016). These optical bands appeared as sharp peaks in the region of 750 and 500 nm, respectively.

The D value is obtained for the perovskite films on the surface of SIF which is higher than that of the perovskite film on the glass surface. A higher surface roughness (R_a) of the silver films is one of the reasons for the higher D value of perovskite films on the surface of SIF. Also as shown in **Figure 5B** and **Supplementary Table S2** an increase in the SIF roughness leads to a decrease in the D value of perovskite films.

In **Figures 5A,B**, the scattering effect was also noticed due to presence of large perovskite particles. This type phenomena was also reported in the reference (Baryshnikova et al., 2020).

Glass substrate was used as a background as the absorption spectra of perovskite films on the surface of SIF were measured (**Figure 5B**). After mathematical subtraction of the island film spectrum from the absorption spectrum of perovskite films on SIF, a local minimum (λ_{Absmin}, **Supplementary Table S3**; **SI**) is formed in the perovskite absorption spectrum in the region of 440–460 nm (**Figure 5**, curve 3), which corresponds to the maximum peak of the absorption spectrum of SIF (**Figure 2B**; **Supplementary Table S2**; **SI**). A different spectrum is formed with a maximum of 630 nm (curve 4, **Figure 6**) after subtracting the perovskite spectrum on the glass from the absorption spectrum of the perovskite film on SIF. It wasn't possible to obtain the resulting spectrum measuring the absorption spectrum of the perovskite film on the surface of SIF (curve 2, **Figure 6**) from summing the absorption spectrum of the perovskite film (curve 1, **Figure 6**) with the absorption spectrum of SIF (curve 5, **Figure 6**). The most likely cause of such changes may be a significant influence of the perovskite film on the properties of the localized plasmon resonance observed on SIF. For silver particles with size much smaller than the wavelength of the excited light ($R << \lambda_{ext.}$), the electrostatic polarizability (α) of NP can be described using the formula (Khlebtsov, 2008):

FIGURE 4 | (A) XRD pattern for the $CH_3NH_3PbI_3$ film. **(B)** A top view SEM image of the $CH_3NH_3PbI_3$ film.

FIGURE 5 | (A) Absorption spectra of perovskite films on glass surface: 1) without annealing; 2) T = 200°C; 3) T = 240°C;4) T = 260°C. The insert shows schematic illustrations ofvalence bands VB1, VB2 and conduction bands CB1 of $CH_3NH_3PbI_3$. **(B)** Absorption spectra of perovskite films on surface with silver island: 1) without annealing; 2) T = 220°C; 3) T = 240°C;4) T = 260°C. The insert shows schematic illustrating energy levels of perovskite and silver films before **(a)** and after **(b)** interaction.

FIGURE 6 | Absorption spectra of perovskite films **(1)** on surface of glass **(2)** on surface with silver island (T = 240°C). Spectrum of perovskite film **(3)** after subtracting the spectrum of the glass substrate with silver island. Difference spectrum **(4)** (curve 2–curve 1) between the perovskite film obtained on the silver surface and on the glass surface. Absorption spectrum **(5)** of the silver island film at T = 240° C.

$$\alpha = 4\pi a^2 \frac{\varepsilon - \varepsilon_m}{\varepsilon + 2\varepsilon_m} \qquad (2)$$

Where, α—electrostatic polarizability of nanoparticles; ε—optical dielectric constant of metal; ε_m—optical dielectric constant of the medium; a–radius of a spherical particle.
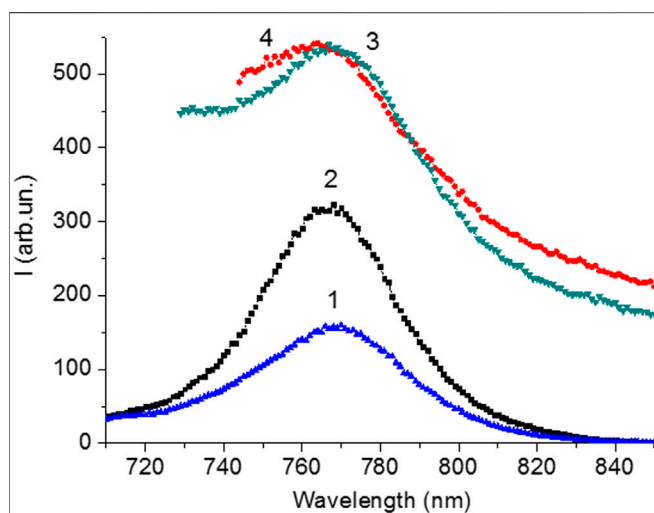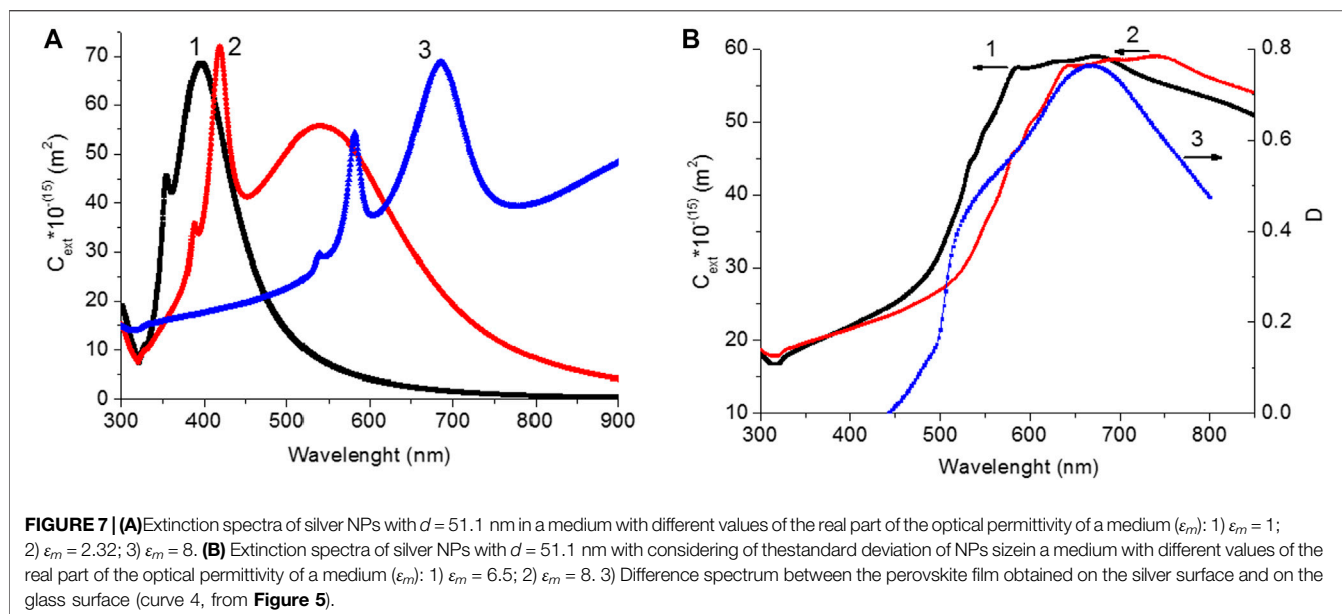
Equation 2 shows that the permittivity of the surrounding environment (ε_m) significantly affects the value of α for the nanoparticle. Parameter α determines the absorption, scattering, and extinction spectra of metal nanoparticles (Khlebtsov, 2008).

The effect of the environment on the absorption spectra of metal nanoparticles is described in reference (Mulvaney, 1996).

The absorption spectra of the nanoparticles were red-shifted with increase of the *KI* shell thickness or the concentration of *I* ions in the solution. Another work investigated the effect of the permittivity of the surrounding environment on the localized plasmon resonance of the metal nanoparticles on a solid substrate surface (Haes et al., 2006; Zhao et al., 2007). However, so far few researches have discussed the influence of the electrical permittivity of perovskite films on the localized plasmon resonance of metal nanoparticles.

$CH_3NH_3PbI_3$ perovskite films have a relatively high value of the real part of the coefficient ε_m ($\varepsilon_m \rightarrow 8$) (Huang, et al., 2017), which is significantly higher than the value of ε_m for air ($\varepsilon_m = 1$) (Ciddor 1996) and cover glass ($\varepsilon_m = 2.32$) (SchottZemax catalog, 2017).

To determine the possible causes of significant changes in the absorption spectra of perovskite films on the silver islands, extinction spectra were simulated for average 51.1 nm of silver NPs in the media with different permittivity values, ε_m, in the range of 1 and 8. The above average size for the SIF was obtained at the annealing temperature of 240°C. Simulation data of the extinction spectra for silver NPs are shown in **Figures 7A,B**. The simulation results show that the extinction spectrum of NPs has redshifts with increasing of the ε_m value. At ε_m = 2.32, the extinction spectrum (curve 2, **Figure 7A**) doesn't differ significantly from the spectrum of silver island with T = 240°C (curve 5, **Figures 2A,B**). The extinction spectra were simulated with uniform size of nanoparticle. In the case of experimental measurements, wide distribution of NPs leads to an increase in the width of its absorption spectrum. Simulation of the extinction spectrum, taking into account the standard deviation from the average size of NPs (**Supplementary Table S1**; **SI**), showed a change in the shape of the spectrum (**Figure 7B**). The possible value of the surrounding nanoparticle's ε_m for the difference spectrum (**Figure 7B**) was estimated. The simulation results are shown in **Figure 7B**, curve 1 and value of ε_m was equal 6.5. This

FIGURE 7 | (A) Extinction spectra of silver NPs with d = 51.1 nm in a medium with different values of the real part of the optical permittivity of a medium (ε_m): 1) ε_m = 1; 2) ε_m = 2.32; 3) ε_m = 8. **(B)** Extinction spectra of silver NPs with d = 51.1 nm with considering of the standard deviation of NPs size in a medium with different values of the real part of the optical permittivity of a medium (ε_m): 1) ε_m = 6.5; 2) ε_m = 8. 3) Difference spectrum between the perovskite film obtained on the silver surface and on the glass surface (curve 4, from **Figure 5**).

FIGURE 8 | Luminescence spectra of $CH_3NH_3PbI_3$ films synthesized on the glass surface **(1, 3)** and on the silver surface **(2, 4)** upon excitation on 400 nm (1, 2) and 550 nm (3, 4).

value is in the range of values for the glass surface ε_m = 2.32 and covered with a perovskite film $\varepsilon_m \rightarrow 8$.

Also, it's necessary to take into account the change in the energy levels and charge of the perovskite film and the silver film during their direct contact (Insert **a,b Figure 5B**).

In order to observe the luminescence of perovskite under optical excitation of various transitions in $CH_3NH_3PbI_3$ (VB1 → CB1 and VB2 → CB1), the luminescence spectra of the perovskite films were measured at the wavelengths of λ_{ext} = 400 and 550 nm (**Figure 8**) (Xing,et al., 2013). The maximum luminescence intensity was found to be between 767–768 nm for all samples, which is listed in **Table 1** with the luminescence excitation wavelengths. The intensity of the emission depends on both

the excitation wavelength and the silver films on the glass samples. An increase in the luminescence intensity of perovskite films is observed in comparison with the luminescence of films on the glass surface (**Figure 8** and **Table 1**) after exciting samples by light with λ = 400 nm. A slight change in the luminescence intensity of perovskite is observed in the case of excitation of this sample by light with λ = 550 nm.

The luminescence kinetics of $CH_3NH_3PbI_3$ films in the nanosecond time range was measured after excited picosecond semiconductor lasers with λ_{gen} = 640 nm (for VB1 → CB1 transition) and with λ_{gen} 488 nm (for VB2 → CB1 transition) (**Figures 9A,B**). Initially, with increase of the annealing temperature, an increase in the average lifetime of the emission (τ_Σ) was observed (**Tables 2, 3**). At the temperature of 220°C, the time τ_Σ started to decrease. The increase in the time τ_Σ is associated with an increase in the proportion of long-term luminescence (τ_2, τ_3) in the integral emission of the perovskite films. The lifetime of the fast component (τ_1) is also increased. There isn't fast component (A_1, τ_1) in the luminescence kinetics of the films with annealing temperatures of 200 and 220°C.

The fast component (τ_1) of the kinetics can be associated with the recombination of charge carriers in the volume of perovskite (bulk recombination). The long-term component (τ_3) is associated with the surface recombination of charge carriers in perovskites. The data show that the presence of silver nanoparticles leads to an increase in the lifetime of recombination luminescence, both in the bulk and surface of the perovskite films. This may be due to a decrease in the rate of non-radiative recombination of charge carriers in perovskite films in the presence of localized plasmon resonance of SIF.

Dong and others (Dong et al., 2018) also discussed an increase of surface recombination lifetime of charge state in the presence of various plasmonic nanostructures. But bulk recombination lifetime didn't change significantly in the presence plasmonic

TABLE 1 | Influence of silver island films on luminescence properties of perovskite films.

| Anneal. temp.°C	Samples	λex. = 400 nm		λex. = 550 нm	
		λ_{max}, nm	$I_{arb.un./D400}$ nm	λ_{max}, nm	$I_{arb.un. ./D550}$ nm
Without annealing	Perovskite—glass	764	47	763	288
	Perovskite—silver	760	28	760	122
180	Perovskite—glass	764	193	764	477
	Perovskite—silver	771	146	771	360
200	Perovskite—glass	771	119	772	462
	Perovskite—silver	763	97	762	253
220	Perovskite—glass	769	136	768	534
	Perovskite—silver	766	131	765	274
240	Perovskite—glass	773	122	773	432
	Perovskite—silver	765	135	765	444
260	Perovskite—glass	765	78	765	533
	Perovskite—silver	769	184	767	353
280	Perovskite—glass	763	51	764	424
	Perovskite—silver	760	34	760	649
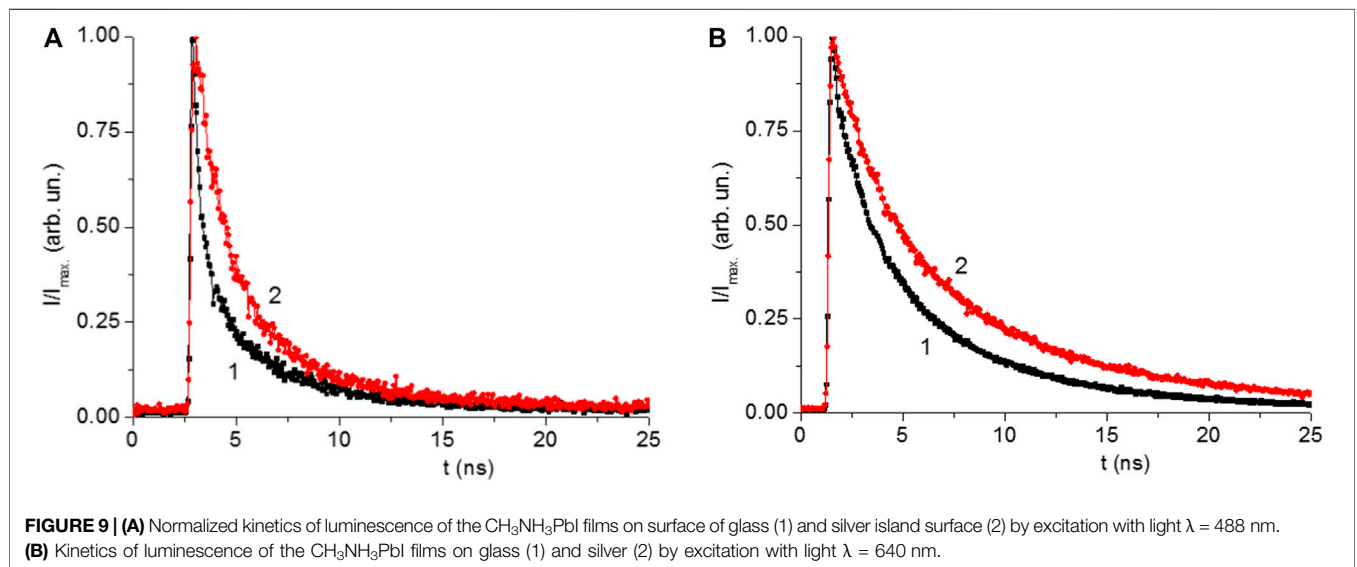
FIGURE 9 | (A) Normalized kinetics of luminescence of the CH_3NH_3PbI films on surface of glass (1) and silver island surface (2) by excitation with light λ = 488 nm. **(B)** Kinetics of luminescence of the CH_3NH_3PbI films on glass (1) and silver (2) by excitation with light λ = 640 nm.

TABLE 2 | Effect of the annealing temperature of silver films on the temporal characteristics of the perovskite films luminescence (λ_{exc} = 488 nm).

Annealing temp. of silver films	D (silver films)	τ_Σ, ns	τ_1, ns	A_1 (%)	τ_2, ns	A_2 (%)	τ_3, ns	A_3 (%)
$CH_3NH_3PbI_3$, without silver films	—	1.71	0.30	50.5	1.76	36.3	8.20	11.2
20°C	0,31	0.941	0.289	51	1,185	43	4,745	6
180°C	0,37	1,732	0.500	38	1,733	47	4,802	15
200°C	0,30	1,411	0.433	44	1,401	45	5,219	11
220°C	0,40	2,655	—	—	1,658	78.6	6,315	21.4
240°C	0,56	2,224	0.729	42	2,262	39	8,881	11
260°C	0,50	1,740	0.545	52	1,945	39	7,380	10
280°C	0,40	1,918	0.299	40	1,300	47	9,095	13

TABLE 3 | Effect of the annealing temperature of silver films on the temporal characteristics of the luminescence of perovskite films (λ_{exc} = 640 nm).

Annealing temp. of silver films	D (silver films)	τ_Σ, ns	τ_1, ns	A_1 (%)	τ_2, ns	A_2 (%)	τ_3, ns	A_3 (%)
$CH_3NH_3PbI_3$, without silver films	—	1,576	0.492	50	2,022	45	8,635	5
20°C	0,31	1,273	0.393	62	1,652	32	8,745	6
180°C	0,37	4,363	1,876	45	4,750	32	8,701	23
200°C	0,30	3,687	0.895	34	2,899	42	8,944	22
220°C	0,40	5,885	—	—	2,836	54.5	9,527	45.5
240°C	0,56	4,820	—	—	2,223	62	9,028	38
260°C	0,50	2,713	0.586	48	2,407	36	9,634	16
280°C	0,40	4,254	1,651	61	5,975	23	11,970	16

nanostructures. Other team also reported (Chirvony et al., 2020) that luminescence lifetime depends on diffusion coefficient of charge carriers and recombination velocities.

CONCLUSION

The optical properties of $CH_3NH_3PbI_3$ perovskite films on the surface of silver island films at different annealing temperatures were studied. Changes in the annealing temperature of silver films lead to changes in the size of silver islands, the surface roughness, and the absorption spectra of these silver films. Studies of the absorption properties of $CH_3NH_3PbI_3$ films on SIF surface indicate a significant influence of perovskite on the properties of localized plasmon resonance in silver nanoparticles. Perovskite films with a higher optical density, D, are formed on the silver surface, which indicates formation of relatively thicker films on the silver surface on contrary to the glass surface. The formation of $CH_3NH_3PbI_3$ thicker films on SIF may be to some degree associated with an increase of surface roughness of the silver films. Comparison of the absorption spectra of SIF before and after deposition of perovskite with the results of numerical calculations of extinction spectra shows a redshift of the absorption spectrum of SIF.

The luminescence intensity of perovskite films depends both on the excitation wavelength of the perovskite film and on the presence SIF on the glass surface. As the perovskite film on the silver films is excited by light at $\lambda_{exc.} = 400$ nm, an increase in the luminescence intensity of perovskite is observed relative to the luminescence of films on the glass surface. In the case of excitation of this sample at $\lambda_{exc} = 550$ nm, a slight change in the luminescence intensity of perovskite is observed.

The study of the kinetics of luminescence decay of perovskite films on the surface of the silver island films indicates that the presence of silver nanoparticles leads to an increase in the lifetime of recombination luminescence, both in the volume of the perovskite film and on its surface. This may ascribe to a decrease in the rate of non-radiative recombination of charge carriers in perovskite films in the presence of localized plasmon resonance of NPs.

Thus, the results obtained show that silver island films can be used to increase the intensity of light emitting diodes based on perovskites. It is indicated by an increase in the luminescence intensity of perovskites on SIF compared to perovskites on glass.

Also, the presence of SIF leads to an increase in the luminescence time of perovskites which can lead to an increase in the lifetime of charge carriers in perovskites and improve the photovoltaic properties of perovskite solar cells.

DATA AVAILABILITY STATEMENT

The original contributions presented in the study are included in the article/**Supplementary Material**, further inquiries can be directed to the corresponding author.

AUTHOR CONTRIBUTIONS

NN oversaw the whole research work and wrote the whole manuscript together with DA and NI. He conducted experiments including synthesis and characterizations of pervoskite nanomaterials. DA did the whole experiments including synthesis of silver and perovskite nanometrails and measurements of luminescence, etc. NI did experiments of Uv-vis absorption spectra with luminescence measurements and joined the experimental results discussion with other two authors. He also wrote the manuscript together with other two authors.

FUNDING

ACKNOWLEDGMENTS

SUPPLEMENTARY MATERIAL

The Supplementary Material for this article can be found online at: https://www.frontiersin.org/articles/10.3389/fmats.2020.600424/full#supplementary-material.

REFERENCES

Afanasyev, D., Ibrayev, N., and Nurmakhanova, A. (2020). Effect of spin-orbit interaction on recombination luminescence of dye in films of halogen-containing derivative poly-N-epoxypropylcarbazole. *J. Photochem. Photobiol. Chem.* 394, 112442. doi:10.1016/j.jphotochem.2020.112442

Afanasyev, D. A., and Ibrayev, N. Kh. (2020). Specific features of photoluminescence of $CH_3NH_3PBI_3$ perovskites synthesized on nanostructured TiO_2 surface. *Optic Spectrosc.* 128 (8), 1108–1114. doi:10.1134/s0030400x20080032

Afanasyev, D. A., Mirzoev, K. Y., and Ibrayev, N. K. (2018). Influence of defects of nanostructured ZnO films on the photovoltaic characteristics of perovskite

solar cells. *IOP Conf. Ser. Mater. Sci. Eng.* 289, 012001, doi:10.1088/1757-899X/289/1/012001

Baryshnikova, K., Gets, D., Liashenko, T., Pushkarev, A., Mukhin, I., Kivshar, Y., et al. (2020). Broadband antireflection with halide perovskite metasurfaces. *Laser Photon. Rev.* 14 (12), 2000338. doi:10.1002/lpor.202000338

Bayles, A., Carretero-Palacios, S., Calió, L., Lozano, G., Calvo, M. E., and Míguez, H. (2020). Localized surface plasmon effects on the photophysics of perovskite thin films embedding metal nanoparticles. *J. Mater. Chem. C* 8, 916–921. doi:10.1039/C9TC05785D

Belykh, V. V., Yakovlev, D. R., Glazov, M. M., Grigoryev, P. S., Hussain, M., Rautert, J., et al. (2019). Coherent spin dynamics of electrons and holes in CsPbBr3 perovskite crystals. *Nat. Commun.* 10 (1–6), 673. doi:10.1038/s41467-019-08625-z

Catchpole, K. R., and Polman, A. (2008). Plasmonic solar cells. *Optic Express* 16 (26), 21793–21800. doi:10.1364/oe.16.021793

Chan, K., Wright, M., Elumalai, N., Uddin, A., and Pillai, S. (2017). Plasmonics in organic and perovskite solar cells: optical and electrical effects. *Advanced Optical Materials* 5, 1600698–1600719. doi:10.1002/adom.201600698

Chirvony, V. S., Sekerbayev, K. S., Pashaei Adl, H., Suárez, I., Taurbayev, Y. T., Gualdrón-Reyes, A. F., et al. (2020). Interpretation of the photoluminescence decay kinetics in metal halide perovskite nanocrystals and thin polycrystalline films. *J. Lumin.* 221 (1–7), 117092. doi:10.1016/j.jlumin.2020.117092

Ciddor, P. E. (1996). Refractive index of air: new equations for the visible and near infrared. *Appl. Optic.* 35, 1566–1573. doi:10.1364/ao.35.001566

Cui, J., Chen, C., Han, J., Cao, K., Zhang, W., Shen, Y., et al. (2016). Surface plasmon resonance effect in inverted perovskite solar cells. *Adv. Sci.* 3 (1–8), 1500312. doi:10.1002/advs.201500312

Dong, H., Lei, T., Yuan, F., Xu, J., Niu, Y., Jiao, B., et al. (2018). Plasmonic enhancement for high efficient and stable perovskite solar cells by employing "hot spots" Au nanobipyramids. *Org. Electron.* 60, 1–8. doi:10.1016/j.orgel.2018.05.030

Duyne, V., Hulteen, R. P., Treichel, J. C., and Treichel, D. A. (1993). Atomic force microscopy and surface-enhanced Raman spectroscopy. I. Ag island films and Ag film over polymer nanosphere surfaces supported on glass. *J. Chem. Phys.* 99 (3), 2101–2115. doi:10.1063/1.465276

Fu, N., Bao, Z. Y., Zhang, Y.-L., Zhang, G., Ke, S., Lin, P., et al. (2017). Panchromatic thin perovskite solar cells with broadband plasmonic absorption enhancement and efficient light scattering management by Au@ Ag core-shell nanocuboids. *Nanomater. Energy* 41, 654–664. doi:10.1016/j. nanoen.2017.10.024

Grainger, R. G., Lucas, J., Thomas, G. E., and Ewen, G. B. (2004). Calculation of mie derivatives. *Appl. Optic.* 43 (28), 5386. doi:10.1364/ao.43.005386

Gu, L., Wen, K., Peng, Q., Huang, W., and Wang, J. (2020). Surface-plasmon-Enhanced perovskite light-emitting diodes. *Small* 16, 2001861–2001919. doi:10. 1002/smll.202001861

Haes, A. J., Zou, S., Zhao, J., Schatz, G. C., Van Duyne, R. P., et al. (2006). Localized surface plasmon resonance spectroscopy near molecular resonances. *J. Am. Chem. Soc.* 128, 10905–10914. doi:10.1021/ja063575q

Han, N., Ji, T., Wang, W., Li, G., Li, Z., Hao, Y., et al. (2019). Boosting the efficiency of quasi two-dimensional perovskite solar cells via an interfacial layer of metallic nanoparticles. *Org. Electron.* 74, 190–196. doi:10.1016/j.orgel.2019. 06.043

Huang, J., Yuan, Y., Shao, Y., and Yan, Y. (2017). Understanding the physical properties of hybrid perovskites for photovoltaic applications. *Nature Rev.* 2 (1–19), 17042. doi:10.1038/natrevmats.2017.42

Khlebtsov, N. G. (2008). Optics and biophotonics of nanoparticles with a plasmon resonance. *Quant. Electron.* 38 (6), 504–529. doi:10.1070/ QE2008v038n06ABEH013829

Krutyakov, Y. A., Kudrinskiy, A. A., Olenin, A. Y., and Lisichkin, G. V. (2008). Synthesis and properties of silver nanoparticles: advances and prospects. *Russ. Chem. Rev.* 77 (3), 233–257. doi:10.1070/rc2008v077n03abeh003751

Li, Y.-F., Kou, Z.-L., Feng, J., and Sun, H.-B. (2020). Plasmon-enhanced organic and perovskite solar cells with metal nanoparticles. *Nanophotonics* 9, 3111–3133. doi:10.1515/nanoph-2020-0099

Moakhar, R. S., Gholipour, S., Masudy-Panah, S., Seza, A., Mehdikhani, A., Riahi-Noori, N., et al. (2020). Recent advances in plasmonic perovskite solar cells. *Adv. Sci.* 7 (13), 1902448. doi:10.1002/advs.201902448

Moniruddin, M., Ilyassov, B., Zhao, X., Smith, E., Serikov, T., Ibrayev, N., et al. 2018). Recent progress on perovskite materials in photovoltaic and water splitting applications. *Mat. Tod. Ener.* 7, 246–259. doi:10.1016/j.mtener. 2017.10.005

Mulvaney, P. (1996). Surface plasmon spectroscopy of nanosized metal particles. *Langmuir* 12 (3), 788–800. doi:10.1021/la9502711

Nuraje, N., and Su, K. (2013). Perovskite ferroelectric nanomaterials. *Nanoscale* 5, 8752–8780. doi:10.1039/c3nr02543h

Oku, T. (2015). "Crystal structures of $CH_3NH_3PbI_3$ and related perovskite compounds used for solar cells," in *Solar cells—new approaches and reviews*. Editors L. A. Kosyachenko (London, UK: IntechOpen), 77–98.

Park, N.-G. (2016). Methodologies for high efficiency perovskite solar cells. *Nano Converg.* 3 (1), 15–13. doi:10.1186/s40580-016-0074-x

Peng, W., Anand, B., Liu, L., Sampat, S., Bearden, B., Malko, A. V., et al. (2016). Influence of growth temperature on bulk and surface defects in hybrid lead halide perovskite films. *Nanoscale* 8, 1627. doi:10.1039/c5nr06222e

Protsenko, I. E., and Uskov, A. V. (2012). Photoemission from metal nanoparticles. *Usp. Fiz. Nauk* 182 (5), 543–554. doi:10.3367/ufnr.0182.201205e.0543

Pydzińska, K., Karolczak, J., Kosta, I., Tena-Zaera, R., Todinova, A., Idígoras, J., et al. (2016). Determination of interfacial charge-transfer rate constants in perovskite solar cells. *ChemSusChem* 9, 1647. doi:10.1002/cssc.201600210

Ribeiro, G. P., Valotto, R. S., de Oliveira, J. P., Guimarães, M. C. C., and Lenz, D. (2020). An inexpensive, automated and reproducible method to conduct quality control in nanoparticles. *Chem. Pap.* 74 (9), 2821–2824. doi:10.1007/s11696-020-01123-3

Rycenga, M., Cobley, C. M., Zeng, J., Li, W., Moran, C. H., Zhang, Q., et al. (2011). Controlling the synthesis and assembly of silver nanostructures for plasmonic applications. *Chem. Rev.* 111, 3669–3712. doi:10.1021/cr100275d

Schaadt, D. M., Feng, B., and Yu, E. T. (2005). Enhanced semiconductor optical absorption via surface plasmon excitation in metal nanoparticles. *Appl. Phys. Lett.* 86 (6), 063106. doi:10.1063/1.1855423

SchottZemax catalog (2017). SchottZemax catalog.

Shabdan, Y., Hanford, B., Ilyassov, B., Dikhanbayev, K., and Nuraje, N. (2018). "Pervoskite solar cell," in *Multifunctional nanocomposites for energy and environmental applications*. Editors Z. Guo, Y. Chen, and N. L. Lu (Weinheim, Germany: Wiley VCH).

Šileikaite, A., Prosycevas, I., Puiso, J., Juraitis, A., and Guobiene, A. (2006). Analysis of silver nanoparticles produced by chemical reducti on of silver salt solution. *Mater. Sci.* 12 (4), 287.

SPCImage 3.9.4. Data Analysis for Fluorescence Lifetime Imaging Microscopy (2012). *SPCImage 3.9.4. Data analysis for fluorescence lifetime imaging microscopy*. Berlin, Germany: Becker &Hickle GmbH.

Stratakis, E., and Kymakis, E. (2013). Nanoparticle-based plasmonic organic photovoltaic devices. *Mater. Today* 16 (4), 133–146. doi:10.1016/j.mattod.2013.04.006

Toropov, N. A., Parfenov, P. S., and Vartanyan, T. A. (2014). Aggregation of cyanine dye molecules in the near fields of plasmonic nanoparticles excited by pulsed laser irradiation. *J. Phys. Chem. C* 118 (31), 18010–18014. doi:10.1021/ jp505234j

Wu, J. L., Chen, F. C., Hsiao, Y. S., Chien, F. C., Chen, P., Kuo, C. H., et al. (2011). Surface plasmonic effects of metallic nanoparticles on the performance of polymer bulk heterojunction solar cells. *ACS Nano* 5 (2), 959–967. doi:10.1021/ nn102295p

Xing, G., Mathews, N., Sun, S., Lim, S. S., Lam, Y. M., Grätzel, M., et al. (2013). Long-range balanced electron- and hole-transport lengths in organic-inorganic $CH_3NH_3PbI_3$. *Science* 342 (6156), 344–347. doi:14.1126/science.1243167

Xing, G., Mathews, N., Lim, S. S., Yantara, N., Liu, X., Sabba, D., et al. (2014). Low-temperature solution-processed wavelength-tunable perovskites for lasing. *Nat. Mater.* 13, 476–480. doi:10.1038/nmat3911

Zhang, W., Saliba, M., Stranks, S. D., Sun, Y., Shi, X., Wiesner, U., et al. (2013). Enhancement of perovskite-based solar cells employing core-shell metal nanoparticles. *Nano Lett.* 13, 4505. doi:10.1021/nl4024287

Zhao, J., Jensen, L., Sung, J., Zou, S., Schatz, G. C., and Duyne, R. P. (2007). Interaction of plasmon and molecular resonances for rhodamine 6G adsorbed on silver nanoparticles. *J. Am. Chem. Soc.* 129, 7647–7656. doi:10.1021/ja0707106